Transition from hydrodynamic flashback to wall-ignition in hydrogen-enriched laminar premixed burners

Hugo Pers, Andrea Aniello, Thierry Schuller

Transition from hydrodynamic flashback to wall-ignition in hydrogen-enriched laminar premixed burners

H. Pers[a,b], A. Aniello[a], T. Schuller[a,c]

[a] *Institut de Mécanique des Fluides de Toulouse, IMFT, Université de Toulouse, CNRS, Toulouse, France*
[b] *Hydrogen Research and Development Laboratory, SERMETA, France*
[c] *Institut Universitaire de France (IUF)*

Abstract

The propensity of hydrogen-enriched flames to flashback poses a challenge when retrofitting natural gas-powered premix burners to accommodate hydrogen. This study investigates how the burner geometry influences the mode of flashback observed in laminar premixed methane/hydrogen-air flames, which are stabilized above slits. Experiments are conducted on a series of 0.6 mm-thick multi-perforated plates with a fixed slit length of 6 mm and widths ranging from 1.0 mm to 0.3 mm. A transparent injection setup facilitates high-speed intensified imaging of the flashback occurrence. Two distinct initiation regimes are identified. The first one designated as 'hydrodynamic' involves upstream flame propagation through a slit, while the second, termed 'wall-ignition', entails autoignition of reactants in contact with the hottest spots of the inner burner wall. Both wall temperature and autoignition delay times are found to be insufficient for distinguishing between the flashback regimes. Instead, an autoignition Damköhler number Da_i comparing a gas residence time to the autoignition delay is used to distinguish the flashback regimes. For $Da_i > 2$, only wall-ignition is observed. For $Da_i < 1$, only hydrodynamic flashback occurs. An intermediate region $1 < Da_i < 2$ where both flashback mechanisms can be triggered is revealed. Finally, reducing the slit width is shown to be ineffective in preventing flashback. Instead, the coupled heat transfer between the flame, burner plate, and fresh gases increases the propensity for wall ignition as the slit width decreases. These findings prompt a reconsideration of the design of hydrogen-enriched premixed laminar burners.

Keywords: FLASHBACK, AUTOIGNITION, PERFORATED PLATE, HYDROGEN SUBSTITUTION, FLAME-WALL INTERACTION, DOMESTIC BURNER
2024 MSC: 00-01, 99-00

Novelty and significance statement

1. Identification of flashback triggered by autoignition of reactants in contact with hot burner walls for hydrogen-enriched flames stabilized on perforated plates.
2. Demonstration of the inadequacy of wall temperature to discriminate between hydrodynamic and autoignition flashback regimes.
3. An autoignition Damköhler number facilitates the differentiation between hydrodynamic and autoignition-induced flashbacks. An intermediate zone where both regimes coexist is also identified.
4. Demonstration of the progressive domination of the autoignition flashback initiation regime as the slit width is reduced, culminating in the disappearance of the hydrodynamically induced flashback regime.

Author contributions

H.P.: designed and performed research, analyzed data, wrote paper draft. A.A.: designed research, reviewed and corrected paper. T.S.: designed research, reviewed and corrected paper.

1. Introduction

Hydrogen is regarded as a promising alternative to fossil fuels [1, 2]. The development of offshore wind farms in northern Europe underscores the promise of Power-to-Gas strategies for converting excess renewable electricity into hydrogen, offering a means of storage and utilization when required [3, 4, 5].
However, the singular combustion characteristics of hydrogen-air flames hinder the conversion of hydrocarbon-based burners to hydrogen [6, 7, 8, 9, 10, 11]. A key issue in laminar premixed systems operating at atmospheric conditions is the high laminar burning velocity S_L [7] of hydrogen/air mixtures which, at stoechiometric conditions, is about 6 times higher than that of a methane-air flame [12]. The disparity between hydrogen and hydrocarbon fuels is further heightened by the low Lewis number of lean hydrogen-air mixtures, resulting in notably faster molecular diffusion of hydrogen species compared to thermal diffusion [13, 14]. It results in a substantial increase in the flame displacement speed near the point of flame anchoring when positively curved towards the fresh reactants [15, 14]. This enhanced flame speed increases the risk of flashback even at bulk velocities significantly surpassing the laminar burning velocity [16, 15]. Furthermore, hydrogen-air flames

are characterized by a small quenching distance [17, 18, 19], allowing flame propagation through narrow openings and facilitating flame stabilization close to the flame-holder. These flame characteristics collectively contribute to enhance heat transfer between the stabilized flames and the walls of the burner, resulting in particularly high burner temperatures. These features increase the propensity of hydrogen flames to flashback upstream within the injection system [6, 20, 21], raising critical safety concerns.

Flashback remains the focal point of many ongoing investigations [14, 22, 23, 24], primarily because of the persistent issues associated to flashback in all premixed systems. The seminal work of Lewis and Von Elbe [25, 26] enabled to identify flashback limits of laminar premixed flames stabilized above burner holes with diameters significantly larger than the flame thickness. They showed that flashback was in this case controlled by the velocity gradient at the burner wall outlet. However, this model does not consider the impact of flame stretch [27, 28, 29, 30], preferential diffusion [31, 32, 33, 34, 35] and coupled heat transfer with the walls [36, 37, 38, 39], the latter being particularly relevant when the size of the burner holes becomes comparable to the flame thickness [40]. It was demonstrated that the combined effects of stretch and preferential diffusion in lean hydrogen air flames significantly reduce their resistance to flashback [14, 16].

In many boilers and material processing burners powered by laminar premixed flames, flame stretch and preferential diffusion were shown to significant modify the stabilization of hydrogen enriched flames above the multi-perforations [6, 41, 42]. In these burners, which operate at near ambient pressure, the fuel-air mixture flows through small slits or holes perforated in a metal sheet above which flames are stabilized. The characteristic size of these openings is less than a millimeter and of the same order of magnitude as the flame thickness and quenching distance of hydrogen flames when reactants are injected at ambient temperature [19]. But the temperature of these slotted burners often exceeds 1000 K, causing substantial preheating of the reactants due to conjugated heat transfer between the flow and the walls [43, 44, 45]. The perforation pattern, material thickness and its thermal properties notably alter the way flames heat the metal and the incoming flow [46, 47, 48, 40].

Conditions leading to flashback for cylindrical multi-perforated burners powered by methane/hydrogen blends were investigated in [6, 20]. It was found that flashback occurs following a thermal transient state after ignition, when the burner wall temperature rises above a threshold value T_w^f. This threshold depends on equivalence ratio ϕ of the mixture and hydrogen hybridization power rate, *i.e.* the fraction of power originating from hydrogen combustion. This temperature can reach values as high as $T_w^f = 1100$ K. In these cases, it has been shown that the critical velocity gradient theory fails to predict the flashback limits [6]. It was then demonstrated that flashback can also be initiated by the autoignition of reactants upstream of the hot flame-holder [20]. These conditions are favored for hydrogen-enriched mixtures as their autoignition delay significantly decreases when exceeding the crossover temperature, which is about $T_c \sim 950$ K for hydrogen-air mixtures. Above this threshold, a chain-branching path progressively takes control of the autoignition kinetics, overriding radical recombination and leading to a sudden H radical concentration growth [49].
Two distinct flashback mechanisms could be identified [20]: (i) hydrodynamic flashback, in which case a flame initially stabilized above a burner perforation propagates upstream through the hole, and (ii) autoignition-induced flashback, triggered by the wall-ignition of the reactants in contact with the hot inner wall of the flame-holder. An autoignition Damköhler number, that compares the residence time of the reactants impinging the perforated plate to the autoignition delay of the mixture, was introduced to differentiate these regimes [50, 51, 52, 53, 54]. Wall-ignition flashbacks could solely be observed for mixtures close to stoichiometry with a limited hydrogen content, which are of limited relevance for future technological advancements compared to lean pure hydrogen air mixtures. For these latter mixtures, flashback only occurred through the hydrodynamic path. These findings were difficult to generalize due to the complex geometry of the cylindrical industrial burner, featuring a series of circular holes and slit perforations of varying sizes and inclinations, including geometrical asymmetries around the burner circumference. Moreover, the burner geometry could not be modified and its influence on flashback was difficult to assess.

The objective of this study is to examine flashback initiation mechanisms under controlled thermal and flow conditions in multi-perforated plates featuring elongated apertures. The conditions leading to hydrodynamic and wall-ignition flashbacks are explored by examining the impact of slit width on these phenomena for a specific burner material, maintaining a constant metal thickness and slit pattern throughout the investigation.
The article is organized as follows. The experimental setup and procedures leading to flashback are first presented. Characterization of the thermal state of the burner and of the temperature of reactants leaving the burner slits is then presented. Flashback initiations and their dynamics are then explored for different burner geometries, unveiling two different regimes depending on slit width and combustible mixture. A criterion that enables to differentiate the different flashback regimes is determined. Finally, conclusions are drawn to clarify the role of the burner geometry on the origin of flashback for H_2-enriched mixtures.

2. Experimental setup and diagnostics

Experiments are carried out on the CHROMA setup (for Comprehension of HydROgen-enriched Mixtures Anomalies), designed to study flashback of laminar premixed flames stabilized on multi-perforated plates.

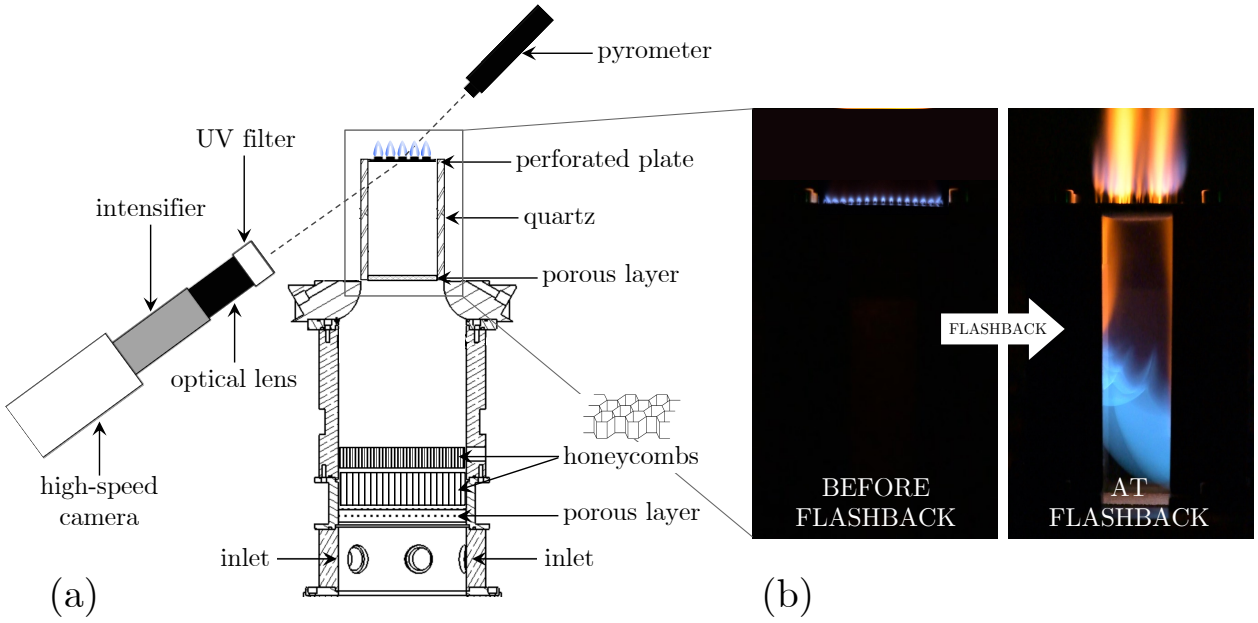

Figure 1: (a): CHROMA experimental setup with the main diagnostics. (b): close-up side view of the square injection chamber during flashback.

Figure 1(a) shows a schematic of the experimental setup and diagnostics used to investigate flashback. A side view of the plate and injection chamber before and during flashback is presented on the right in Fig. 1(b). Square perforated plates are fixed on top of a transparent injection chamber made of four 8 mm-thick fused silicate windows, which are maintained vertically by four steel mounts (Fig. 1(b)). The transparent windows provide optical access to the bottom of the perforated plates, enabling to follow the motion of the flame during its propagation through the injection holes in the event of flashback. The 35 mm-wide transparent square injection chamber is positioned above a converging nozzle, that provides a smooth transition from a 100 mm diameter cylindrical plenum to the transparent injection unit section. The plenum is supplied with methane-hydrogen/air mixtures at atmospheric pressure and ambient temperature. Two bronze porous layers with a 40 µm pore size and a 4 mm thickness serve as flame-arrestors. One is placed at the upstream end of the transparent chamber, another one is positioned upstream of the cylindrical plenum. Honeycombs in the cylindrical plenum are used to homogenize the flow.

The flow rates are monitored with Bronkhorst F-201CV mass flow controllers with a precision of ±0.5% of the desired mass flow rate and 0.1% of the full scale. In the worst-case scenario, this leads to an uncertainty on equivalence ratio of ±0.02 for pure hydrogen. The uncertainty on repeatability, however, remains below 0.2% of the desired mass flow rate. The hydrogen and methane purity is > 99.99%, and air is dehumidified. A pressure relief valve is fitted in the plenum and set to open when the over-pressure exceeds 1 bar.

Six perforated plates described in Tab. 1 are tested. Figure 2 shows a schematic of perforated plate B with the main

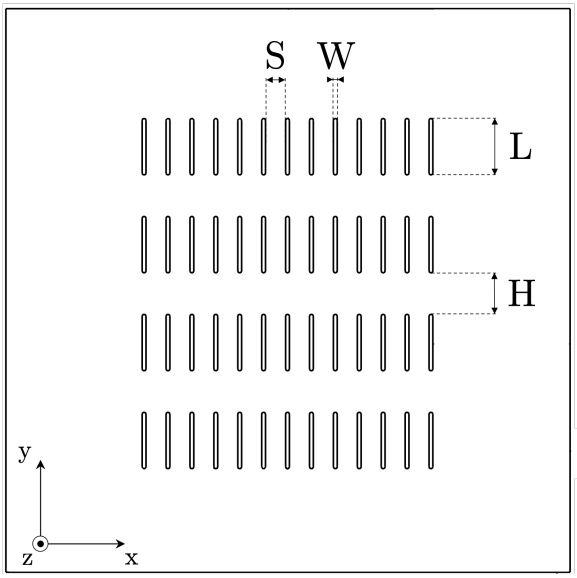

Figure 2: Top-view of slit-perforated plate B with the main dimensions.

dimensions. All plates consist of $e = 0.6$ mm thick square sheets of refractory steel 18SR with 59 mm side length. They are perforated by a periodical pattern of slits. The slit length L, the gap H between two rows of slits and the spacing S between columns of slits are kept constant, as numerous studies highlighted the significant impact of slit pattern on both flame stabilization and thermal state of the burner [14, 47, 46, 48, 40]. They are respectively fixed to $L = 6$ mm, $H = 4$ mm and $S = 2$ mm. Only the slit width is varied between $W = 1.00$ mm (plate O) and 0.32 mm (plate E). plate O serves as reference. The slits edges are rounded to form an oblong shape of radius

$R = W/2$.

Table 1: Perforated plates geometrical characteristics.

Plate	W (mm)	S (mm)	H (mm)	L (mm)	A_s (mm^2)	N_s	A_t (mm^2)
O	1.00	2	4	6	5.79	36	208
A	0.80	2	4	6	4.66	44	205
B	0.58	2	4	6	3.41	52	177
C	0.42	2	4	6	2.48	52	129
D	0.37	2	4	6	2.19	60	131
E	0.32	2	4	6	1.90	60	114

Slit dimensions were selected to cover hole dimensions of industrial multi-perforated burners [6, 16, 20, 41, 48]. The dimensions indicated in Tab. 1 are measured with macro-photography. The number of slits N_s of each plate is adapted as the slit width W changes, to limit variations of the total open flow cross-section area $A_t = N_s A_s$, where the cross section area of a single slit is given by $A_s = W(L - W) + \pi(W/2)^2$. The slit length is limited to $L = 6$ mm. Longer slits could not be tested as they led to a bending of the metal at high temperatures, limiting the burner operability. It is interesting to determine the hydraulic diameter of the slits investigated. For plate D with slit width $W_D = 0.37$ mm, one finds $D_h \approx 2LW/(L+W) = 0.7$ mm. This value is comparable to the diameters of holes of the domestic cylindrical burner examined in [20], for which both hydrodynamic and wall-ignition flashback could be identified.

Plate O with the largest slit width $W_O = 1.00$ mm is only used to illustrate flashback propagation as the associated light signal is more intense in this case, providing sharper images. The slit width $0.32 \leq W \leq 1.00$ mm should be compared to the quenching diameter d_Q that prevents the propagation of flames through a hole. For a pure hydrogen/air mixture at $\phi = 0.7$ and ambient temperature $T_0 = 300$ K, Jung et al. [19] found $d_Q \simeq 0.75$ mm using an annular stepwise diverging tube. Plates with larger slits are therefore expected to be more sensitive to flashback triggered by flame propagation through the slit opening, while the smaller ones are more likely to quench the flame.

2.1. Flame imaging

A Nikon D8500 camera equipped with a 105 mm lens is used to take color images of the flames. Flashback initiation is scrutinized with a high-speed Phantom TMX 7510 camera paired with a LaVision IRO X intensifier and a Nikkor 105 mm UV lens. A 305-315 nm bandpass filter is used to only capture the OH^* emission signal [55], thereby obtaining the location of the reaction front of the laminar premixed flames [49]. The high-speed camera is positioned at a 30° angle relative to the horizontal plane of the perforated plate as shown in Fig. 1 to ensure a large field of view of its inner surface during flashback.

2.2. Temperature measurements

After ignition, the small flames stabilized close to the metal cause a rapid increase of the metal temperature T_w, leading in turn to an elevation of the temperature T_u of reactants exiting the slits, reaching much higher values than their initial temperature $T_0 = 300$ K when injected inside the plenum. The plate temperature T_w is measured with a bichromatic infrared pyrometer (FLUKE Endurance Series, precision of $\pm 0.5\% + 2^o$C), capable of detecting surface temperatures between 250 and 1200 ^{o}C. The temperature T_w is obtained from the signal emitted by a 4 mm diameter target spot on the external side of the plate. Measurements of the metal wall temperature were also conducted with the pyrometer beam focused on the upstream side of the burner. Since the metal is thin ($e = 0.6$ mm) and highly conductive, the Biot number is small enough to consider that the temperature within the metal remains constant across its thickness. For these latter measurements, there is no flame or burned gas in the line of sight of the detector, and no bias due to thermal radiation. These measurements carried out below the plate yielded results close, within 10 K, to those taken from the top, corroborating the adequacy of measuring the burner temperature T_w from the top, which was easier to set up.

Direct measurement of the temperature T_u of the mixture exhausting from the slits is challenging due to the small dimensions of perforations and the high temperature T_w of the wall. Placing a small thermocouple inside the slit while stabilizing a flame would significantly disrupt the flow and modify flame stabilization, besides being greatly affected by radiative transfer. While the metal can be deemed isothermal across its 0.6 mm thickness, reactants undergo substantial preheating as they flow along the wall and cross the slits.

Therefore, the preheat temperature T_u is determined with the same technique as the one described in [6, 20, 56], and its accuracy is assessed in the present case. The burner is first ignited at a stable operating condition. After reaching thermal equilibrium between flame, wall and gases, the fuel supply is stopped at instant t_0 while keeping the air flow rate constant. At instant t_1, a 1.5 mm K-type thermocouple is placed in the hot gas stream above the central slit indicated by the black arrow in Fig. 3.1 to measure the decrease of reactant gas temperature with time for instants $t \geq t_1$. Influence of wall thermal radiation on this gas temperature measurement was demonstrated to be negligible in [20]. The preheat temperature of the mixture before flame extinction is deduced by extrapolating the exponential decrease back to the instant t_0 of flame extinction [56].

Examples of experimental data gathered for operating conditions $\phi = 0.70$ and $PH_2 = 60\%$ for plate D, and $\phi = 0.80$ and $PH_2 = 65\%$ for plate E are plotted in Fig. 3. In this figure, T_u is averaged from several independent measurements, with a relative difference of approximately ±3% between the different samples, indicating the good repeatability of measurements.

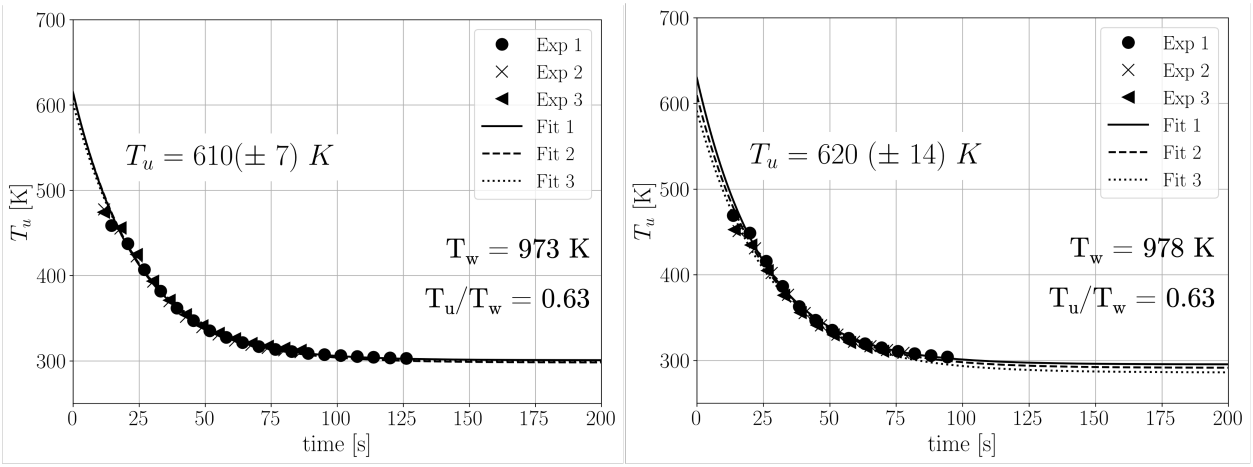

(a) plate D, $\phi = 0.70$, $PH_2 = 60\%$

(b) plate E, $\phi = 0.80$, $PH_2 = 65\%$

Figure 3: Evolution with time of the preheat temperature of the combustible mixture exiting the burner slits for two operating conditions. The initial preheat temperature T_u is inferred from extrapolation to time $t = 0$ s. The wall temperature T_w is 973 K (left) and 978 K (right), leading to $T_u/T_w \simeq 0.63$ in both cases.

2.3. Experimental methodology

The different cases explored are compared based on the mean value of the bulk flow velocity U_b at temperature T_u inside a single slit:

$$U_b(T_u) = \frac{\dot{m}}{\rho_u A_t} = \frac{\dot{m}}{\rho_u A_s N_s} \quad (1)$$

where $\dot{m}$ is the total mass flow rate of reactants injected inside the burner, ρ_u the density of the preheated mixture at T_u, N_s the total number of slits and A_s the cross-section area of a single slit.

A systematic procedure is followed to analyze the causes of flashback for the investigated perforated plates and H_2/CH_4-air mixtures. Fuels and air mass flow rates are first adjusted to reach the desired hydrogen power fraction PH_2, equivalence ratio ϕ and total thermal power P. The burner is then ignited by approaching a blowtorch above the slits. After ignition, three scenarios are possible:

- STABLE: If the temperature of the plate T_w reaches a stable asymptotic value and no flashback is observed for at least 5 minutes, the operational state is categorized as stable.
- FB-H and FB-AI: If a flame stabilizes above the slits and the plate temperature T_w increases until reaching a threshold and then faces flashback for a plate temperature T_w^f, flashback initiation is investigated to determine its origin. In case of an upstream flame propagation through a slit, the condition is categorized as FB-H (FlashBack induced Hydrodynamically). If flashback is triggered by autoignition of reactants in contact with the hot wall, the condition is classified as FB-AI (Autoignition induced FlashBack).
- FB-IN: If flashback occurs instantaneously at ignition while the plate is still cold, the condition is categorized as FB-IN (FlashBack occuring INstantaneously). In these cases, it was checked that flashback is always due to upstream flame propagation through the slits, *i.e.* corresponds to a particular case of FB-H. The dynamics spanning from the initial flame kernel to flashback is beyond the scope of this study. Interested readers are referred to [57].

After each test, the burner is cooled down and is only re-ignited once the quartz windows of the injection square chamber, featuring the highest thermal inertia of the system, have cooled down back to ambient temperature T_0. All experiments presented in this work are made at constant power per unit surface of slit area, $P_s \simeq 4.3\,\mathrm{MW\,m^{-2}}$, meaning that the ratio of bulk flow velocity to laminar burning velocity $(U_b/S_L)_{T_0}$ at temperature T_0 through a slit remains constant for a given mixture composition. The power density is only changed in the last Sec. 3.5 to verify the impact on FB-AI of the residence time of reactants in the vicinity of the wall.

3. Results and discussion

Figure 4 shows a side view of flames above plate B (W_B = 0.58 mm), taken with the Nikon D8500 camera at 60 fps. The equivalence ratio and total thermal power are kept constant at $\phi = 0.68$ and $P = 2.0$ kW, while the power fraction of hydrogen is increased from $PH_2 = 30\%$ to $PH_2 = 97\%$, in which case flashback is reached. In Figs. 4(a-c), the flame is stable and its height decreases as the hydrogen fraction in the mixture increases. The instant following flashback at $PH_2 = 97\%$ is captured in Fig. 4(d). The light trails are caused by the fast expulsion of microscopic metal particles. The yellow jets exiting the slits result from the blow-off of remaining flames due to the large pressure wave caused by flashback inside the burner.

The side view in Figs. 4(a-c) indicates that the flow rate is well distributed between the different slits with symmetric

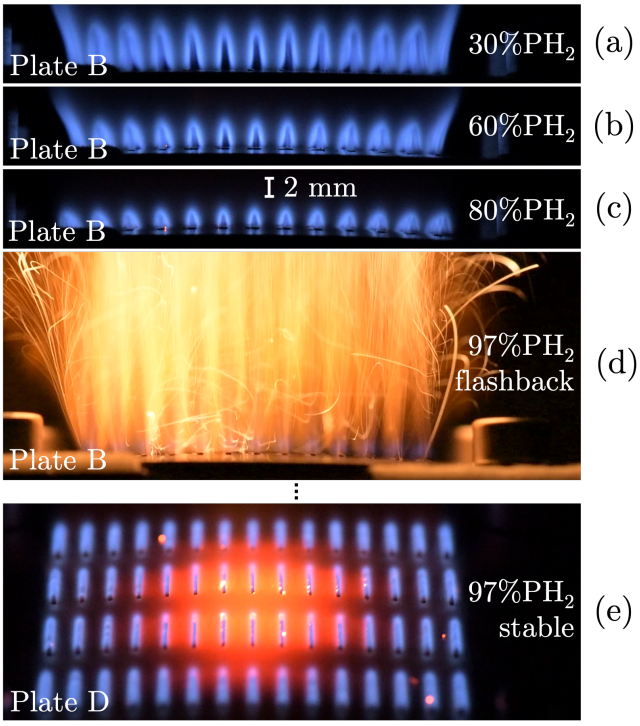

Figure 4: Side view of flames above plate B (W_B = 0.58 mm) with ϕ = 0.68, P = 2.0 kW, for different H_2-hybridization rates PH_2 = 30% (a), PH_2 = 60% (b), PH_2 = 80% (c), and during flashback at PH_2 = 97% (d). (e): oblique view of flames above plate D (W_D = 0.37 mm) for ϕ = 0.68, P = 1.5 kW, PH_2 = 97%.

flame patterns. At the edges, however, the plate temperature substantially drops because of heat losses, and the external branch of the flames can be blown off in Figs. 4(a-b). However, these slits are never involved in flashback initiation, which invariably occurs through a slit within the hotter central region of the plate. Furthermore, close to flashback as in Fig. 4(c), flames are well stabilized above all slits and present a symmetrical shape, as also confirmed by the oblique view of the burner in Fig. 4(e).

Figure 4(e) shows flames stabilized on plate D for the same mixture equivalence ratio, hybridization rate and power density as in Fig. 4(d). Due to its narrower slit width W_D = 0.37 mm than plate B with W_B = 0.58 mm, the flames are now stable. The red hot region in the center of the plate is due to thermal radiation of the metal and indicates how the temperature is distributed over the burner surface. This image confirms that the temperature rapidly decreases towards the sides due to heat losses at the plate edges.

3.1. Thermal characterization

The wall temperature distribution is further characterized in Fig. 5 for plate D, at P = 0.57 kW, ϕ = 0.80 and PH_2 = 60%. Temperature profiles are examined along two perpendicular lines crossing at the center of the plate. The measurement locations are colored based on their temperature. The temperature profiles along the x and y axes are displayed on the sides of the figure. The temperature distribution has a parabolic

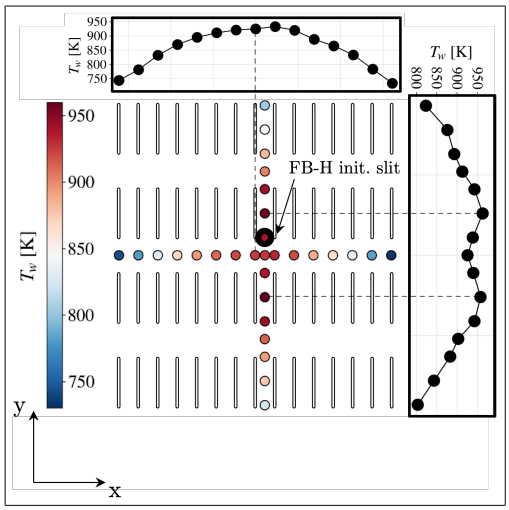

Figure 5: Evolution of the wall temperature T_w for plate D at P = 0.57 kW, ϕ = 0.80, PH_2 = 60% along two orthogonal directions. Measurement spots are colored by the measured wall temperature. Temperature profiles are also reported for each direction in the top and right plots. The black spot indicates the location selected to determine T_w in this study. The slit through which FB-H flashback is preferentially triggered is indicated by the black arrow.

shape along the x-axis, dropping by over 150 K between the center and the edge of the plate. Nevertheless, within the five central columns, the wall temperature remains roughly uniform with relative variations below 3%. The temperature distribution along the y-axis exhibits two local maxima in the middle of the space between parallel slits. The temperature in the center of the plate is slightly smaller due to the absence of flame in x-direction. However, the temperature barely changes along the two central rows with relative variations below 4%.

These experiments allow for the delineation of a region corresponding roughly to the two most central rows and five most central columns with a relatively uniform wall temperature. In this central area, the flow is uniform and flames are symmetric (Fig. 4). The high wall temperature makes this area a preferential location for flashback initiation as confirmed by flame images shown in Fig. 6. The only value retained for the wall temperature T_w in the following is the one measured between central slits, next to the central row spacing, as outlined by the black disk in Fig. 5.

The preheat temperature T_u of reactants exiting the slit shown by the arrow in Fig. 5 is compared to the wall temperature T_w at the black disk in the same figure. For each plate, three operating conditions are considered. Table 2 indicates that the ratio between T_u and T_w remains roughly constant for a given plate geometry, with relative differences below 4%. This corroborates previous measurements made in [6, 20] on a different setup and leads to the empirical correlation for the ratio T_u/T_w in the last column of Tab. 2, valid at $P_s \simeq 4.3\,\mathrm{MW\,m^{-2}}$ and for T_w between 850 K and 1100 K. It is worth noticing that the ratio T_u/T_w increases abruptly from

Table 2: Evolution of T_u as a function of T_w for plates A to E.

Plate	Power (kW)	ϕ	PH_2 (%)	T_w (K)	T_u (K)	T_u/T_w	
	0.90	0.80	49	863	400	0.46	
A	0.90	0.85	44	893	403	0.45	0.46
	0.90	0.85	40	978	491	0.46	
	0.78	0.80	45	934	480	0.51	
B	0.78	0.85	40	903	460	0.51	0.51
	0.78	0.90	36	978	491	0.50	
	0.57	0.70	70	838	452	0.54	
C	0.57	0.80	60	963	500	0.52	0.53
	0.57	0.85	55	1008	520	0.52	
	0.57	0.70	60	973	610	0.63	
D	0.57	0.75	55	1003	621	0.62	0.62
	0.57	0.80	50	993	617	0.62	
	0.50	0.70	80	960	596	0.62	
E	0.50	0.80	65	979	620	0.63	0.62
	0.50	0.85	55	978	600	0.61	

0.53 to 0.62 between plate C with slit width $W_C = 0.42$ mm and plate D featuring slit width $W_D = 0.37$ mm.

3.2. Flashback dynamics

The high-speed UV intensified imaging setup is employed with a field of view focused on the inner surface in the center of the plate. Examples of flashback initiation and propagation associated to FB-H and FB-AI mechanisms are presented in Fig. 6. Videos can be found online as supplementary material. The initiation location is zoomed in for better visualization.

Figure 6(a) illustrates flashback occurring on plate O characterized by the largest slit width $W_0 = 1.0$ mm for an equivalence ratio $\phi = 0.60$, a hydrogen hybridization rate $PH_2 = 90\%$ and a global power $P = 1.4$ kW. The wall temperature close to flashback location is $T_w = 873$ K. Before flashback, the flame front that is stabilized above the outer surface of the burner can barely be distinguished through the slit in the first image at $t = 0.0$ ms. At flashback, however, a bright spot appears distinctly in the images at instants $t = 0.1$ ms and $t = 0.2$ ms with a flame propagating upstream through the central slit. This case therefore belongs to FB-H. It must be underlined that the flame displacement through the slit is always initiated at the oblong extremity of the slit. Figure 6(b) is depicting a flashback event for plate D, with a slit width $W_D = 0.37$ mm, taking place for $\phi = 0.75$, $PH_2 = 79\%$ and $P = 0.57$ kW. In this case, flashback is triggered by the autoignition of reactants at the wall and corresponds to FB-AI.In line with the hottest spot located in the center of the plate, autoignition occurs between the two central rows and columns of slits for all the FB-AI cases studied.

These observations confirm the existence of FB-H and FB-AI, endorsing the fact that FB-AI is not limited to the specific geometry of the domestic cylindrical burner studied in [20].

The subsequent section explores the impact of slit width on these flashback regimes.

3.3. Influence of slit width

Flashback initiation is studied for perforated plates B, D and E operating at a constant power density $P_s \simeq 4.3\,\mathrm{MW\,m^{-2}}$ through the slits. Figure 7 maps the different flashback regimes observed when slit width W is reduced, as a function of equivalence ratio ϕ and hydrogen hybridization power rate PH_2. Crosses correspond to FB-AI and circles denote FB-H. Additional details and results for other plate geometries can be found in the supplementary material.

Stable operation can only be achieved at the bottom left corners in Fig. 7 for lean conditions with a limited H_2 hybridization rate, independently of the width W of the slits. For plate B with slit width $W_B = 0.58$ mm, flashback also occurs instantaneously after ignition (FB-IN) for highly H_2-enriched mixtures close to stoichiometry in the upper right corner in Fig. 7(a). The domain in between the STABLE and FB-IN regions corresponds to flashback taking place at a given temperature threshold T_w^f, during the thermal transient state after ignition. The slit width of plate B is large enough to allow the upstream propagation of the flame through the slit and FB-H is triggered in all cases.

Figure 7(b) shows results for plate D. Reducing the slit width to $W_D = 0.37$ mm enables to avoid instantaneous flashback (FB-IN) over the whole operating domain, meaning that the slit width is small enough to quench the flame at the cold wall after ignition. But this resistance to flashback weakens as the plate temperature increases. A reduction of the slit width W is accompanied by a further increase of the temperature T_u of the reactants crossing the slits. Table 2 indicates that for a wall at $T_w \simeq 1000$ K, the reactants preheat temperature goes from $T_u = 520$ K for plate C to $T_u = 620$ K for plate D. This large temperature gap leads to a 40% increase of the laminar burning velocity from $S_L(T_u) = 3.7$ m/s to 5.2 m/s, causing the flames to stabilize closer to the wall, which in turn heats up even more. Associated to the fact that the flame cannot freely propagate through the slit because of quenching, flashback can only occur in small slits at much higher temperatures.

In Fig. 7(b), FB-H and FB-AI co-exist in the upper-right corner. FB-H predominantly occurs in highly hydrogen-enriched lean mixtures, whereas FB-AI is observed at richer conditions for mixtures with a lower hydrogen content, $PH_2 \leq 80\%$. The delimitation between these flashback regimes is difficult to appraise. When $PH_2 \simeq 80\%$, a slight increase in hydrogen hybridization rate leads to a switch from FB-AI towards FB-H. This hinders the distinction between these cases, as discussed below in Sec. 3.4.

Figure 7(c) shows results for plate E when the slit width is further reduced to $W_E = 0.32$ mm. As for plate D, the small slit width prevents FB-IN flashbacks occurrence after ignition. It also prevents flame propagation through the slit even at high temperature, causing FB-H regimes to disappear. However, the operability domain with stable flames for plate E does not widen compared to plate D. Stable regions are only shifted and flashback is now fully driven by FB-AI. For this burner, all flashbacks take place with wall temperatures exceeding $T_w > 1050$ K.

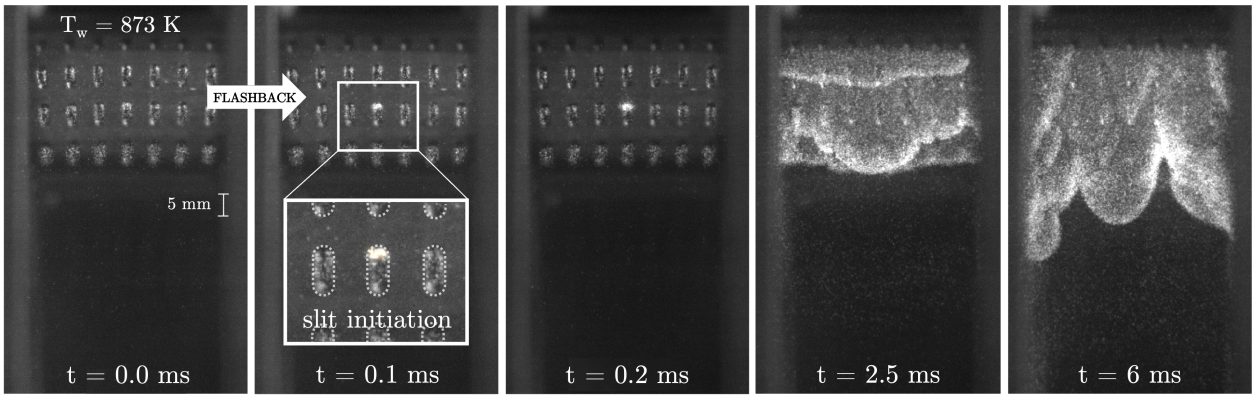

(a) plate 0, W = 1.0 mm, ϕ = 0.60, PH_2 = 90%, 1.40 kW

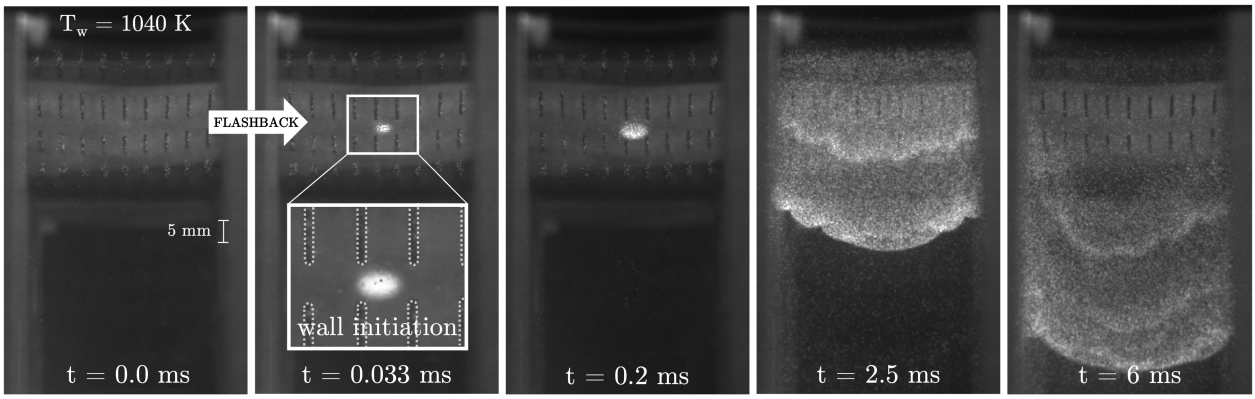

(b) plate D, W = 0.37 mm, ϕ = 0.75, PH_2 = 79%, 0.57 kW

Figure 6: High-speed imaging of flashback initiation and propagation, for (a) hole initiation FB-H and (b) wall initiation FB-AI. T_w is the wall temperature at the center of the plate. Slits are outlined by a dotted line in the zoomed insert.

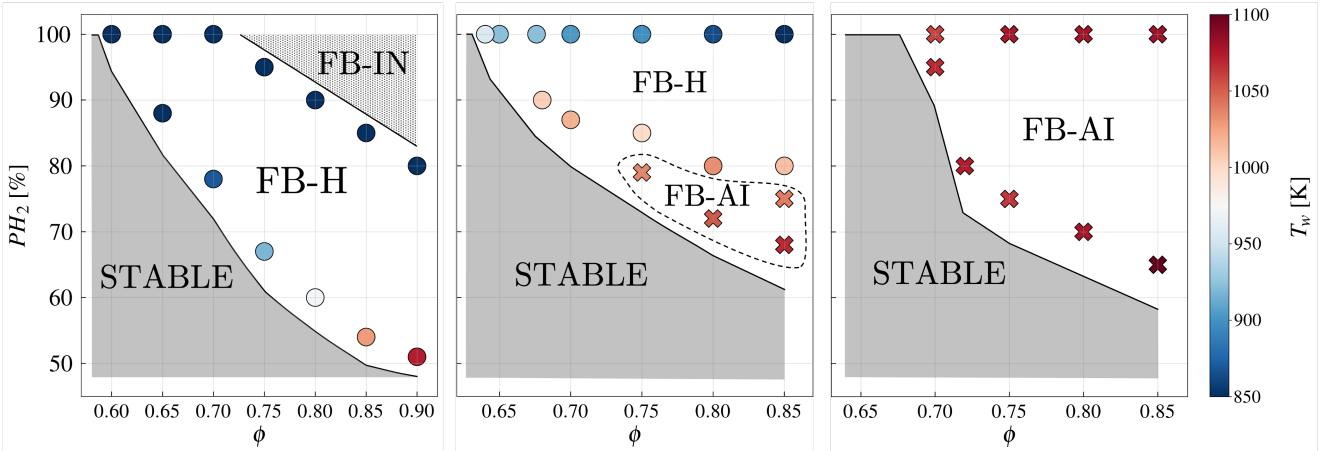

Figure 7: Stabilization maps as a function of equivalence ratio ϕ and hydrogen hybridization power rate PH_2. Flashback conditions are colored by the wall temperature threshold T_w^f. The power density through perforations remains constant at $P_s \simeq 4.3\,\mathrm{MW\,m^{-2}}$. (a) plate B, W_B = 0.58 mm, P = 0.78 kW. (b) plate D, W_D = 0.37 mm, P = 0.50 kW. (c) plate E, W_E = 0.32 mm, P = 0.57 kW. Crosses: FB-AI. Circles: FB-H.

These experiments confirm that reducing the size of the burner holes does not increase flashback resistance. Nevertheless, it leads to the disappearance of instantaneous flashback FB-IN just after ignition and provides a better resistance to hydrodynamic flashback FB-H. In smaller slits, the reactants are further preheated by the hot wall and flames stabilize

closer to the burner, resulting in elevated wall temperatures that promote the onset of wall-ignition flashback FB-AI. The distinction between the two flashback regimes is now further examined.

3.4. Distinction between FB-H and FB-AI

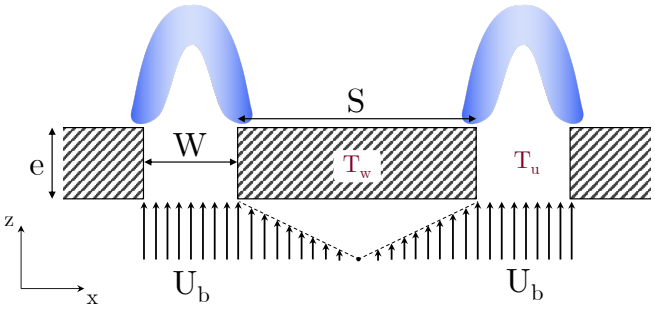

Figure 8: Model of the perforated plate burner in (x, z) plane used to determine the residence time τ_r of the reactants below the hot wall at T_w.

To determine whether autoignition can take place for a given mixture, bulk velocity and wall temperature, the Damköhler number Da_i introduced in [20] is used to compare the residence time τ_r of the reactants in contact with the wall to the autoignition delay time τ_i of the combustible mixture.
Figure 8 is depicting a model of the flow interaction with the hot burner wall at T_w. The bulk velocity of the reactants in the slits calculated at the preheat temperature T_u at which flashback occurs is denoted $U_b(T_u)$. In this model, it is assumed that streamlines in Fig. 8 split symmetrically between the two slits. Furthermore, the model considers that the reactants impinge the wall over a distance $S/2$ at an average speed $U_b(T_u)/2$, under the assumption that the flow velocity decreases linearly from the slit to the midpoint of the space between slits at $S/2$. While this is admittedly a rough approximation, it effectively incorporates the primary flow and geometric characteristics of the flow-wall interaction. Consequently, under these conditions, the residence time is given by $\tau_r = S/U_b(T_u)$ and the Damköhler can be expressed as follows:

$$Da_i = \frac{\tau_r}{\tau_i} = \frac{1}{\tau_i(T_w)} \frac{S}{U_b(T_u)} \tag{2}$$

In this expression, autoignition delays $\tau_i(T_w)$ are calculated using a constant volume batch reactor using the CANTERA solver for mixtures at $p = 1$ atm and assuming temperature T_w with the GRI-MECH 3.0 mechanism.

The Damköhler numbers calculated at flashback limits for all plates are presented in Fig. 9 as a function of the ratio of bulk velocity to laminar burning velocity (U_b/S_L). On the left, in Fig. 9(a), results are presented when (U_b/S_L) is determined for the temperature $T_0 = 300$ K of reactants injected inside the burner. On the right, in Fig. 9(b), this ratio is determined for the preheat temperature T_u at which the mixture leaves the slits. The symbols in these plots are colored by the wall temperature T_w.

The data in Figs. 9(a-b) show that all conditions associated to wall-ignition FB-AI flashback (symbols with black edges in the figure) are at the top left corner and all conditions associated to FB-H hydrodynamic flashback appear at the bottom right corner, with a smooth transition between the two regimes. To interpret these results, it is necessary to examine the mechanisms altering the flow velocity and the flame displacement speed. The effects of preferential diffusion and the ability of the wall to quench the flame play a crucial role here.
For the plates with the largest slits, i.e plate A and to some extent plate B, the Damköhler number remains well below unity, and the velocity ratio (U_b/S_L) at both T_0 and T_u takes large values up to 4. There are two main reasons for this behavior. First, lean mixtures with a high hydrogen content are characterized by a Lewis number well below unity and a flame displacement speed S_d close to the flame root much higher than the laminar burning velocity S_L [13, 14]. Hydrodynamic flashback was shown to be triggered in these cases at velocity ratios much higher than unity, $(U_b/S_L) \gg 1$ [15, 16]. Additionally, the impact of flame quenching also needs to be considered. Jung et al. [19] reported a quenching width $d_Q \approx 0.75$ mm for lean H_2-air flames at $\phi = 0.7$ and ambient temperature $T_u = T_0 = 300$ K. For plate A with a slit width $W_A = 0.80$ mm slightly larger than $d_Q = 0.75$ mm, lean hydrogen flames can propagate through the slit immediately after ignition without being quenched. For plate B with a slit width $W_B = 0.58$ mm smaller than $d_Q = 0.75$ mm, the flame is unable to propagate through a cold slit at $T_w = T_0$ except for mixtures close to stoichiometry with a high hydrogen content (see the top right corner in Fig. 7). For other conditions, the flame stabilizes downstream the slits and progressively heats up the plate. This increase in wall temperature T_w causes a rise of the preheat temperature T_u of the mixture, reducing the ratio $(U_b/S_L)_{T_u}$ because the laminar burning velocity S_L increases faster with T_u than the bulk flow velocity U_b does [58]. In parallel, the higher preheat temperature T_u leads to a decrease of the flame quenching distance d_Q [59, 60, 61], eventually allowing the flame to flashback through the slit, although at higher temperatures T_u and smaller velocity ratios $(U_b/S_L)_{T_u}$ than for larger slits. This mechanism explains the shift of $(U_b/S_L)_{T_u}$ values as the slit width is reduced from $W_A = 0.80$ mm for plate A to $W_B = 0.58$ mm for plate B and $W_C = 0.42$ mm for plate C. Concurrently, the surge in wall temperature T_w that comes with slit width reduction eventually makes wall-ignition possible if the residence time of the reactants is large enough. This is for example the case for plate C when the autoignition Damköhler number exceeds 2 in Fig. 9.

For small slits or small shares of hydrogen, the ratio $(U_b/S_L)_{T_0}$ at flashback decreases and the associated Damköhler number increases in Fig. 9(a). In this plot, the trend depends on the slit width. However, when results are plotted as a function of $(U_b/S_L)_{T_u}$, that takes into account the preheat temperature T_u of the reactants leaving the slits, flashback limits collapse in Fig. 9(b) on a single curve common to all considered plates for wall temperatures higher than $T_w = 950$ K. One can

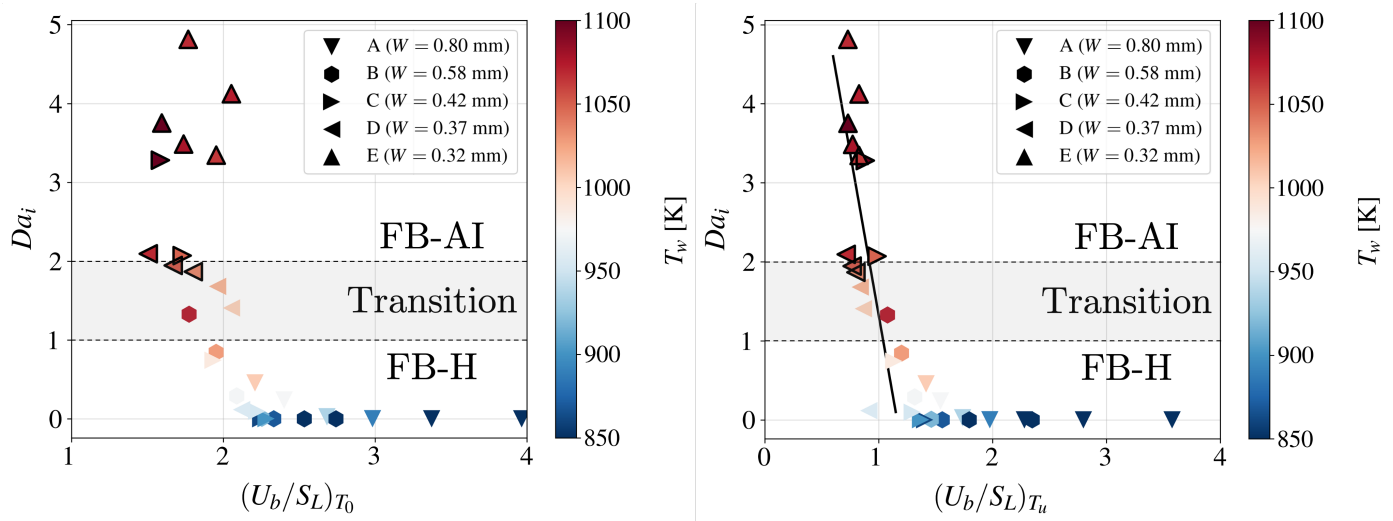

(a) U_b and S_L calculated at T_0

(b) U_b and S_L calculated at $T_u = f(T_w)$

Figure 9: Evolution of the autoignition Damköhler number Da_i as a function of U_b/S_L for reactants at temperature T_0 (a) and T_u (b). FB-AI are indicated by symbols with black edges.

also identify a threshold around $(U_b/S_L)_{T_u} \sim 1$. Below this threshold, the only possible way to flashback is an abrupt increase of the Damköhler number with wall-ignition FB-AI, with a trend common to all considered plates.

Three regions associated to different values of the Damköhler number can be delimited:

- For Damköhler numbers $Da_i < 1$, only upstream flame propagation FB-H flashback is triggered. The wall temperature remains generally below $T_w < 950$ K, but can exceed in some cases $T_w > 1000$ K for flashback of mixtures close to stoichiometry with a limited content of hydrogen.
- For Damköhler numbers $Da_i > 2$, flashback is always triggered by wall-ignition FB-AI of the reactants below the plate. The wall temperature is above $T_w > 1050$ K in almost all cases.
- For intermediates values of the Damköhler number $1 < Da_i < 2$, both FB-H and FB-AI can be triggered, with FB-AI initiations featuring slightly larger Da_i values than any FB-H initiations. This co-existence is mainly observed for plate D with slit width $W_D = 0.37$ mm.

It is important to note that the threshold values of Da_i determined in this study are intended to assist in identifying the transition from FB-H to FB-AI regimes, rather than to be directly used as guidelines for burner design.
A sensitivity analysis, detailed in the supplementary material section, explores the influence of uncertainties in wall temperature measurements on the observed nature of the flashback event. It is concluded that the results in Fig. 9 remain marginally affected, so that the smooth transition of the Damköhler number between FB-H and FB-AI cannot be attributed to inadequate temperature measurements. This smooth transition contrasts with the clear distinction between FB-H and FB-AI regimes based on values of Da_i that was reported for the industrial burners studied in [20]. This prompts a reevaluation of the pertinence of Da_i in distinguishing FB-H and FB-AI, compared to a simple criterion based on the temperature T_w of the plates. This problem is addressed in the next section by analyzing the impact of the hydrogen hybridization rate on these transitions.

3.5. Impact of hydrogen hybridization rate

Figure 10(a) shows the influence of mixture temperature taken at the wall temperature T_w and hybridization rate PH_2 on autoignition delay time τ_i of CH_4/H_2-air mixtures, calculated using Cantera with GRIMECH 3.0 mechanism. In the range $0.6 \leq \phi \leq 0.9$, the equivalence ratio barely alters the autoignition delay time of hydrogen-air mixtures (less than 2%). The impact is also limited for CH_4/H_2 blends, remaining below 9% for PH_2=50% at $T_w = 1000$ K (not shown).
The observed drop in autoignition delay between 920 K and 970 K is linked to the crossover temperature of hydrogen-air mixtures $T_c \simeq 950$ K, which was found to play a key role in triggering the FB-AI regime in [20, 62]. Drops of the same order of magnitude are observed for H_2-enriched CH_4/air mixtures, down to $PH_2 = 50\%$. However, above $T_w \simeq 970$ K, the decrease of τ_i with temperature is much slower. Figure 10(a) shows that the temperature needed to reach a sub-millisecond threshold (e.g. 0.3 ms) significantly depends on PH_2.
Figure 10(b) illustrates this effect by presenting, as a function of PH_2, the wall temperature T_w corresponding to an autoignition delay $\tau_i = 0.3$ ms. This specific duration is selected because, for

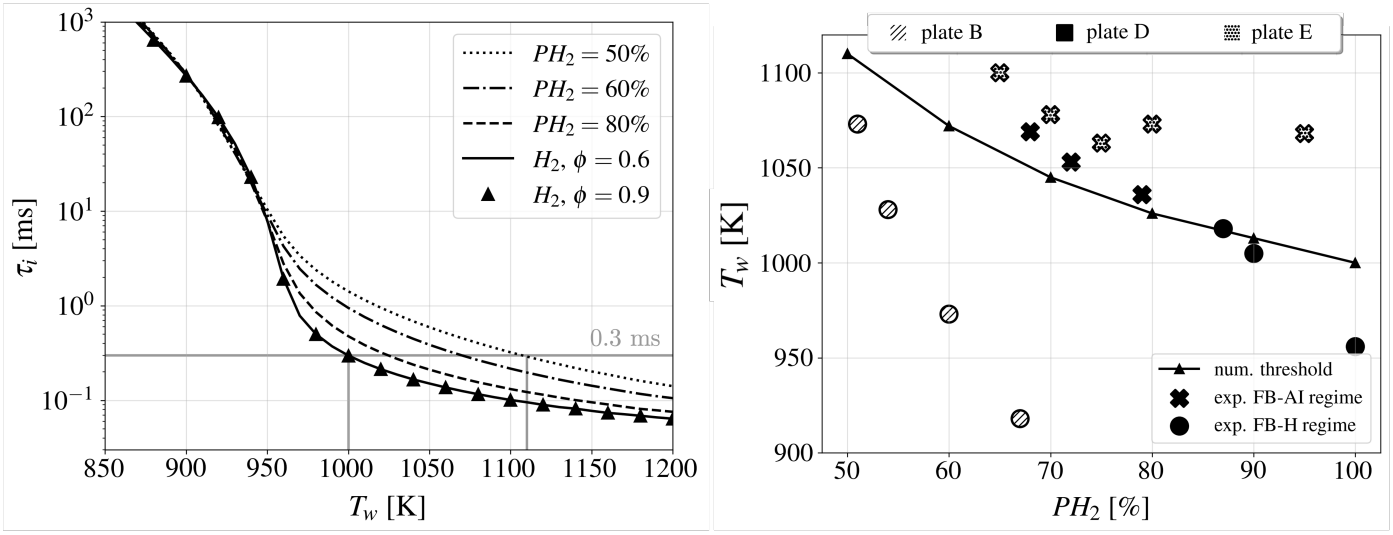

(a) Autoignition delay

(b) Temperature

Figure 10: (a) Autoignition delay of CH_4/H_2-air mixtures as a function of temperature and hybridization rate for two equivalence ratios $\phi = 0.6$ and 0.9. Grey lines: $\tau_i = 0.3$ ms and associated mixture temperatures for $PH_2 = 100\%$ and $PH_2 = 50\%$. (b) Temperatures T_w needed to obtain an autoignition delay time $\tau_i \leq 0.3$ ms at $\phi = 0.6$ as a function of the hybridization power rate PH_2. Flashback limits are reported for plate B (hatched symbols), plate D (filled symbols) and plate E (dotted symbols). FB-AI: crosses. FB-H: circles.

the reference plates and flow conditions explored, the condition $Da_i \sim 2$ corresponds to $\tau_i \sim 0.3$ ms.

The difference of wall temperature needed to reach $\tau_i = 0.3$ ms is $\Delta T_w = 110$ K, varying from $T_w = 1110$ K for $PH_2 = 50\%$ to $T_w = 1000$ K for $PH_2 = 100\%$. Wall temperatures T_w measured at flashback limit for plates B, D and E are also reported in Fig. 10(b). All conditions corresponding to FB-AI lie above the threshold $\tau_i = 0.3$ ms, while FB-H are below this threshold. This explains the absence of FB-AI regimes for plate B ($W_B = 0.58$ mm) even for wall temperatures reaching $T_w = 1075$ K, because of a too limited hydrogen content PH_2. These results confirm that the wall temperature T_w alone cannot be used to discriminate the occurrence of FB-AI.

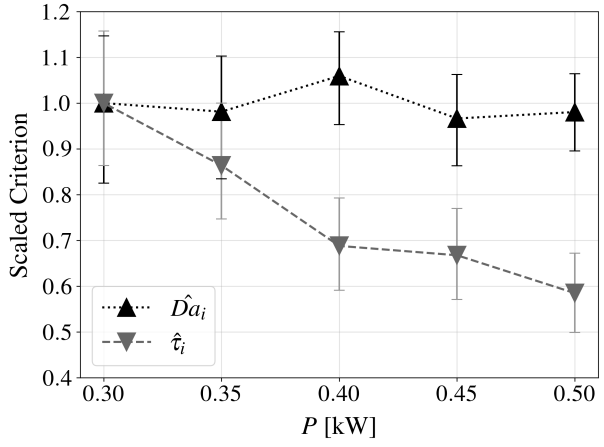

Figure 11: Relative variation of Da_i and τ_i at flashback as a function of thermal power. $\hat{Da}_i = Da_i/(Da_i(0.3\ kW)$, $\hat{\tau}_i = \tau_i/(\tau_i(0.3\ kW))$. plate E, $\phi = 0.70$, $PH_2 = 100\%$.

To assess the role of the residence time τ_r of the reactants in the vicinity of the hot wall, additional experiments are conducted with plate E, for which the only observed regime is FB-AI, at $\phi = 0.70$ and $PH_2 = 100\%$. The thermal power is here progressively increased by 40% in order to alter τ_r.

The evolution of Da_i and τ_i with thermal power is plotted in Fig. 11. In this figure, values for Da_i and τ_i are scaled by their respective values $Da_i = 3.28$ and $\tau_i = 0.24$ ms at the minimum $P = 0.3$ kW. While the Damköhler number at which flashback occurs remains roughly constant, the ignition time delay τ_i needed to trigger flashback drops by about 40% as the power is increased by 40%. These results corroborate that wall-ignition is controlled by the competition between the gas residence time below the plate and the autoignition delay, *i.e.* the Damköhler number, rather than by the sole autoignition delay.

4. Conclusion

Flashback mechanisms of H_2-enriched flames have been experimentally investigated on canonical multi-perforated plates presenting slits width between 1.00 mm and 0.32 mm.

Two regimes of flashback initiation, one due to an upstream flame propagation through a slit (FB-H) and the other triggered by autoignition of reactants below the plate (FB-AI), have been identified after the thermal transient state that follows burner ignition. For a fixed power density, these different mechanisms leading to flashback have been shown to depend on mixture equivalence ratio, hydrogen hybridization rate, burner geometry and wall temperature with an increasing propensity to trigger autoignition-induced flashback as the slit width is reduced.

An autoignition Damköhler number Da_i comparing the autoignition delay of the reactants in contact with the hot wall with the residence time of these reactants has been used to

differentiate the flashback regimes. It has been shown that Da_i is a function of the ratio of bulk velocity to laminar burning velocity at the temperature T_u of the mixture leaving the slit, $(U_b/S_L)_{T_u}$, that presents a threshold around $(U_b/S_L)_{T_u} \simeq 1$ below which a huge increase of Da_i is necessary to reach flashback. Flashback initiation has been shown to be triggered by FB-AI for $Da_i > 2$ and by FB-H for $Da_i < 1$, with a transition zone for $1 < Da_i < 2$ where both regimes can be observed.

As the slit width decreases, hydrodynamically initiated FB-H flashbacks gradually disappear, yet the resistance to flashback remains unchanged due to the rise in plate temperature, thereby promoting wall-ignition FB-AI. Eventually, it becomes the sole flashback mechanism for particularly narrow slits, with autoignition substituting to FB-H even under lean pure hydrogen conditions.

These conclusions may lead to rethink the development of hydrogen-enriched premixed laminar burners, as even lean pure hydrogen flame are found to be limited by autoignition, which was shown to make slit or hole size reduction ineffective to prevent flashback.

Acknowledgments

This project received support and funding from the SERMETA Research and Development Laboratory, as well as funding from the Association Nationale Recherche Technologie (ANRT) through the CIFRE grant n° 2021/1069. This project has received funding from European Research Council (ERC) under the European Union's HORIZON research and innovation programme (SCIROCCO, Grant agreement No. 832248 and SELECT-H, Grant agreement No. 101097984). Finally, the development of the experimental setup would not have been possible without the help of S. Cazin, G. Albert, S. Lun and L. Mouneix. Special thanks to J. Eydoux who manufactured the perforated plates.

References

[1] S. Griffiths, B. K. Sovacool, J. Kim, M. Bazilian, J. M. Uratani, Industrial decarbonization via hydrogen: A critical and systematic review of developments, socio-technical systems and policy options, Energy Res Soc Sci 80 (2021) 102208.

[2] T. Capurso, M. Stefanizzi, M. Torresi, S. Camporeale, Perspective of the role of hydrogen in the 21st century energy transition, Energ Convers Manage 251 (2022) 114898.

[3] R. Winkler-Goldstein, A. Rastetter, Power to gas: the final breakthrough for the hydrogen economy?, Green 3 (2013) 69–78.

[4] H. Blanco, A. Faaij, A review at the role of storage in energy systems with a focus on power to gas and long-term storage, Renew Sust Energ Rev 81 (2018) 1049–1086.

[5] G. Gahleitner, Hydrogen from renewable electricity: An international review of power-to-gas pilot plants for stationary applications, Int J Hydrogen Energy 38 (2013) 2039–2061.

[6] A. Aniello, T. Poinsot, L. Selle, T. Schuller, Hydrogen substitution of natural-gas in premixed burners and implications for blow-off and flashback limits, Int J Hydrogen Energy 47 (2022) 33067–33081.

[7] F. Halter, C. Chauveau, I. Gökalp, Characterization of the effects of hydrogen addition in premixed methane/air flames, Int J Hydrogen Energy 32 (2007) 2585–2592.

[8] D. R. Jones, W. A. Al-Masry, C. W. Dunnill, Hydrogen-enriched natural gas as a domestic fuel: an analysis based on flash-back and blow-off limits for domestic natural gas appliances within the uk, Sustain Energy Fuels 2 (2018) 710–723.

[9] H. de Vries, A. V. Mokhov, H. B. Levinsky, The impact of natural gas/hydrogen mixtures on the performance of end-use equipment: Interchangeability analysis for domestic appliances, Appl Energ 208 (2017) 1007–1019.

[10] H. de Vries, H. B. Levinsky, Flashback, burning velocities and hydrogen admixture: Domestic appliance approval, gas regulation and appliance development, Appl Energ 259 (2020) 114116.

[11] Y. Zhao, V. McDonell, S. Samuelsen, Influence of hydrogen addition to pipeline natural gas on the combustion performance of a cooktop burner, Int J Hydrogen Energy 44 (2019) 12239–12253.

[12] G. Yu, C. Law, C. Wu, Laminar flame speeds of hydrocarbon+ air mixtures with hydrogen addition, Combust Flame 63 (1986) 339–347.

[13] V. Kurdyumov, E. Fernandez-Tarrazo, Lewis number effect on the propagation of premixed laminar flames in narrow open ducts, Combust Flame 128 (2002) 382–394.

[14] F. Vance, L. de Goey, J. van Oijen, Development of a flashback correlation for burner-stabilized hydrogen-air premixed flames, Combust Flame 243 (2022) 112045.

[15] E. Flores-Montoya, A. Aniello, T. Schuller, L. Selle, Predicting flashback limits in H_2 enriched CH_4/air and C_3H_8/air laminar flames, Combust Flame 258 (2023) 113055.

[16] F. Fruzza, R. Lamioni, L. Tognotti, C. Galletti, Flashback of H_2-enriched premixed flames in perforated burners: Numerical prediction of critical velocity, Int J Hydrogen Energy 48 (2023) 31790–31801.

[17] M. Fukuda, K. Korematsu, M. Sakamoto, On quenching distance of mixtures of methane and hydrogen with air., Bull. JSME 24 (1981) 1192–1197.

[18] Z. Liu, N. I. Kim, An assembled annular stepwise diverging tube for the measurement of laminar burning velocity and quenching distance, Combust Flame 161 (2014) 1499–1506.

[19] Y. Jung, M. J. Lee, N. I. Kim, Direct prediction of laminar burning velocity and quenching distance of hydrogen-air flames using an annular stepwise diverging tube (asdt), Combust Flame 164 (2016) 397–399.

[20] H. Pers, A. Aniello, F. Morisseau, T. Schuller, Autoignition-induced flashback in hydrogen-enriched laminar premixed burners, Int J Hydrogen Energy 48 (2023) 10235–10249.

[21] T. García-Armingol, J. Ballester, Operational issues in premixed combustion of hydrogen-enriched and syngas fuels, Int J Hydrogen Energy 40 (2015) 1229–1243.

[22] V. Hoferichter, C. Hirsch, T. Sattelmayer, Prediction of confined flame flashback limits using boundary layer separation theory, J Eng Gas Turbines Power 139 (2017) 021505.

[23] T. B. Kıymaz, E. Böncü, D. Güleryüz, M. Karaca, B. Yılmaz, C. Allouis, İskender Gökalp, Numerical investigations on flashback dynamics of premixed methane-hydrogen-air laminar flames, Int J Hydrogen Energy 47 (2022) 25022–25033.

[24] R. Ranjan, N. T. Clemens, Insights into flashback-to-flameholding transition of hydrogen-rich stratified swirl flames, Proc. Combust. Inst. 38 (2021) 6289–6297.

[25] B. Lewis, G. V. Elbe, Stability and structure of burner flames, J Chem Phys 11 (1943) 75–93.

[26] G. V. Elbe, M. Mentser, Further studies of the structure and stability of burner flames, J Chem Phys 13 (1945) 89–100.

[27] C. Law, Dynamics of stretched flames, Symp. (Int.) Combust. 22 (1989) 1381–1402.

[28] G. D. Álamo, F. A. Williams, A. L. Sánchez, Hydrogen-oxygen induction times above crossover temperatures, Combust Sci Technol 176 (2004) 1599–1626.

[29] K. Aung, M. Hassan, G. Faeth, Effects of pressure and nitrogen dilution on flame/stretch interactions of laminar premixed $H_2/O_2/N_2$ flames, Combust Flame 112 (1998) 1–15.

[30] D. W. Mikolaitis, The interaction of flame curvature and stretch, part 1: The concave premixed flame, Combust Flame 57 (1984) 25–31.

[31] F. H. Vance, P. de Goey, J. A. van Oijen, The effect of thermal diffusion on stabilization of premixed flames, Combust Flame 216 (2020) 45–57.

[32] M. Mizomoto, Y. Asaka, S. Ikai, C. Law, Effects of preferential diffusion on the burning intensity of curved flames, Symp. (Int.) Combust. 20

(1985) 1933–1939.
[33] C. Sun, C.-J. Sung, L. He, C.-K. Law, Dynamics of weakly stretched flames: quantitative description and extraction of global flame parameters, Combust Flame 118 (1999) 108–128.
[34] L. Berger, A. Attili, H. Pitsch, Intrinsic instabilities in premixed hydrogen flames: Parametric variation of pressure, equivalence ratio, and temperature. part 1 - dispersion relations in the linear regime, Combust Flame 240 (2022) 111935.
[35] L. Berger, A. Attili, H. Pitsch, Intrinsic instabilities in premixed hydrogen flames: parametric variation of pressure, equivalence ratio, and temperature. part 2 – non-linear regime and flame speed enhancement, Combust Flame 240 (2022) 111936.
[36] F. Dabireau, B. Cuenot, O. Vermorel, T. Poinsot, Interaction of flames of $H_2 + O_2$ with inert walls, Combust Flame 135 (2003) 123–133.
[37] K. Kedia, H. Altay, A. Ghoniem, Impact of flame-wall interaction on premixed flame dynamics and transfer function characteristics, Proc. Combust. Inst. 33 (2011) 1113–1120.
[38] C. Jainski, M. Rißmann, B. Böhm, J. Janicka, A. Dreizler, Sidewall quenching of atmospheric laminar premixed flames studied by laser-based diagnostics, Combust Flame 183 (2017) 271–282.
[39] H. Kosaka, F. Zentgraf, A. Scholtissek, C. Hasse, A. Dreizler, Effect of flame-wall interaction on local heat release of methane and dme combustion in a side-wall quenching geometry, Flow Turbul Combust 104 (2020) 1029–1046.
[40] H. Pers, P. Masset, E. Flores-Montoya, L. Selle, T. Schuller, Influence of slit asymmetry on blow-off and flashback in methane/hydrogen laminar premixed burners, Combust Flame 263 (2024) 113413.
[41] R. Lamioni, C. Bronzoni, M. Folli, L. Tognotti, C. Galletti, Feeding H_2-admixtures to domestic condensing boilers: Numerical simulations of combustion and pollutant formation in multi-hole burners, Appl Energ 309 (2022) 118379.
[42] A. M. Gamal, A. H. Ibrahim, E.-M. M. Ali, F. M. Elmahallawy, A. Abdelhafez, M. A. Nemitallah, S. S. Rashwan, M. A. Habib, Structure and lean extinction of premixed flames stabilized on conductive perforated plates, Energy Fuels 31 (2017) 1980–1992.
[43] K. S. Kedia, A. F. Ghoniem, Mechanisms of stabilization and blowoff of a premixed flame downstream of a heat-conducting perforated plate, Combust Flame 159 (2012) 1055–1069.
[44] H. Yang, Y. Feng, X. Wang, L. Jiang, D. Zhao, N. Hayashi, H. Yamashita, Oh-plif investigation of wall effects on the flame quenching in a slit burner, Proc. Combust. Inst. 34 (2013) 3379–3386.
[45] V. Kornilov, R. Rook, J. ten Thije Boonkkamp, L. De Goey, Experimental and numerical investigation of the acoustic response of multi-slit bunsen burners, Combust Flame 156 (2009) 1957–1970.
[46] H. M. Altay, K. S. Kedia, R. L. Speth, A. F. Ghoniem, Two-dimensional simulations of steady perforated-plate stabilized premixed flames, Combust Theory Model 14 (2010) 125–154.
[47] F. H. Vance, Y. Shoshin, L. de Goey, J. A. van Oijen, An investigation into flashback and blow-off for premixed flames stabilized without a recirculation vortex, Combust Flame 235 (2022) 111690.
[48] R. Lamioni, C. Bronzoni, M. Folli, L. Tognotti, C. Galletti, Effect of slit pattern on the structure of premixed flames issuing from perforated burners in domestic condensing boilers, Combust Theory Model 27 (2023) 218–243.
[49] A. L. Sánchez, F. A. Williams, Recent advances in understanding of flammability characteristics of hydrogen, Prog Energy Combust Sci 41 (2014) 1–55.
[50] N. Donohoe, A. Heufer, W. K. Metcalfe, H. J. Curran, M. L. Davis, O. Mathieu, D. Plichta, A. Morones, E. L. Petersen, F. Güthe, Ignition delay times, laminar flame speeds, and mechanism validation for natural gas/hydrogen blends at elevated pressures, Combust Flame 161 (2014) 1432–1443.
[51] R. K. Cheng, A. K. Oppenheim, Autoignition in methanehydrogen mixtures, Combust Flame 58 (1984) 125–139.
[52] C. Trevino, F. Méndez, Asymptotic analysis of the ignition of hydrogen by a hot plate in a boundary layer flow, Combust Sci Technol 78 (1991) 197–216.
[53] L. Boeck, J. Melguizo-Gavilanes, J. Shepherd, Hot surface ignition dynamics in premixed hydrogen–air near the lean flammability limit, Combust Flame 210 (2019) 467–478.
[54] J. Melguizo-Gavilanes, L. Boeck, R. Mével, J. Shepherd, Hot surface ignition of stoichiometric hydrogen-air mixtures, Int J Hydrogen Energy 42 (2017) 7393–7403.
[55] R. W. Schefer, W. D. Kulatilaka, B. D. Patterson, T. B. Settersten, Visible emission of hydrogen flames, Combust Flame 156 (2009) 1234–1241.
[56] Y. Ding, D. Durox, N. Darabiha, T. Schuller, Chemiluminescence of burner-stabilized premixed laminar flames, Combust Sci Technol 191 (2019) 18–42.
[57] T. Yahou, T. Schuller, J. R. Dawson, The effect of ignition procedure on flashback of hydrogen-enriched flames, Proc. ASME Turbo Expo 86953 (2023) V03AT04A039.
[58] A. Kalantari, V. McDonell, Boundary layer flashback of non-swirling premixed flames: Mechanisms, fundamental research, and recent advances, Prog Energy Combust Sci 61 (2017) 249–292.
[59] H. Kosaka, F. Zentgraf, A. Scholtissek, L. Bischoff, T. Häber, R. Suntz, B. Albert, C. Hasse, A. Dreizler, Wall heat fluxes and CO formation/oxidation during laminar and turbulent side-wall quenching of methane and DME flames, Int J Heat Fluid Flow 70 (2018) 181–192.
[60] C. Hasse, M. Bollig, N. Peters, H. Dwyer, Quenching of laminar iso-octane flames at cold walls, Combust Flame 122 (2000) 117–129.
[61] T. Zirwes, T. Häber, F. Zhang, H. Kosaka, A. Dreizler, M. Steinhausen, C. Hasse, A. Stagni, D. Trimis, R. Suntz, et al., Numerical study of quenching distances for side-wall quenching using detailed diffusion and chemistry, Flow Turbul Combust 106 (2021) 649–679.
[62] F. A. Williams, Combustion theory, CRC Press, 2018.